FORECASTERS' FORUM

A Single-Column Method to Identify Sea and Land Breezes in Mesoscale-Resolving NWP Models

CHRISTOFFER HALLGREN,[a] HEINER KÖRNICH,[b] STEFAN IVANELL,[a] AND ERIK SAHLÉE[a]

[a] *Department of Earth Sciences, Uppsala University, Uppsala, Sweden*
[b] *Swedish Meteorological and Hydrological Institute, Norrköping, Sweden*

(Manuscript received 14 September 2022, in final form 12 April 2023, accepted 17 April 2023)

ABSTRACT: One of the most prominent mesoscale phenomena in the coastal zone is the sea-breeze/land-breeze circulation. The pattern and its implications for the weather in coastal areas are well described, and with mesoscale-resolving operational NWP models the circulation can be captured. In this study, a straightforward method to identify sea and land breezes based on the change in wind direction in the column above a grid point on the coastline is presented. The method was tested for southern Sweden using archived output from the HARMONIE-AROME model with promising results, describing both the seasonal and diurnal cycles well. In areas with a complex coastline, such as narrow straits, the concept of the land–sea breeze becomes less clear, and several ways to address this problem for the suggested method are discussed. With an operational index of the sea and land breezes, the forecaster can better understand and express the weather situation and add value for people in the coastal zone. Further, the indices can be used to study systematic biases in the model and to create climatologies of the sea and land breezes.

SIGNIFICANCE STATEMENT: A wind pattern that is frequently occurring in the coastal zone is the sea-breeze/land-breeze circulation, and the purpose of this study is to test a new method to automatically identify sea breezes and land breezes in weather forecasts. Knowing if a sea breeze or a land breeze is occurring is helpful for the operational weather forecaster in understanding the weather situation. It can also be used to study systematic model behavior, for example, errors in the forecast temperature during sea-breeze conditions. The method has been tested for seven coastal sites in Sweden and shows promising results both in case studies and multiyear statistics.

KEYWORDS: Sea breezes; Mesoscale processes; Mesoscale forecasting; Operational forecasting

1. Introduction

Forecasting the weather in the coastal zone has always been a challenge for meteorologists as the sharp gradients of atmospheric variables and the drastic change in surface properties give rise to internal boundary layers and mesoscale phenomena. Among these mesoscale effects, the one that is probably best described and has been studied the most is the sea breeze; see Fig. 1 for a textbook example of the sea-breeze circulation. For a complete review of sea-breeze formation and different aspects of the phenomenon, we refer to Simpson (1994) and Miller et al. (2003).

In brief, as the solar radiation rapidly heats the land surface during daytime, a convective atmospheric boundary layer is created. The water surface does not warm as fast due to the higher heat capacity of water compared to the one of land. Consequentially, the land-side convection will generate a pressure gradient force directed from water toward land, resulting in an onshore advection of air. This wind, the sea breeze, strengthens as the temperature difference between the land and sea surfaces increases throughout the day and as the convection over land intensifies. Also, as the wind speed increases the wind direction starts to change as a consequence of the Coriolis effect (e.g., Neumann 1977). Simultaneously, as the air flows from the sea sector toward land at lower levels, a return flow is established higher up in the boundary layer with winds in the opposite direction. As the sea breeze brings cooler maritime air over the land, it takes some time (i.e., distance from the coast) before this air has been heated and starts to rise. Thus, convective clouds are not formed at the immediate coast, but rather several kilometers inland, referred to as the sea-breeze front.

During the evening transition, when the land surface cools faster than the sea surface, with subsiding air creating stable conditions over land, the sea-breeze circulation reverses. This circulation is commonly known as the land breeze. The land-breeze circulation is typically shallower and less pronounced than the sea-breeze circulation and winds are weaker (Miller et al. 2003, see also Holmer and Haeger-Eugensson 1999). In synoptic situations with a dominant wind, the sea breeze can act to decrease or increase the wind speed at different heights.

Denotes content that is immediately available upon publication as open access.

Corresponding author: Christoffer Hallgren, christoffer.hallgren@geo.uu.se

DOI: 10.1175/WAF-D-22-0163.1

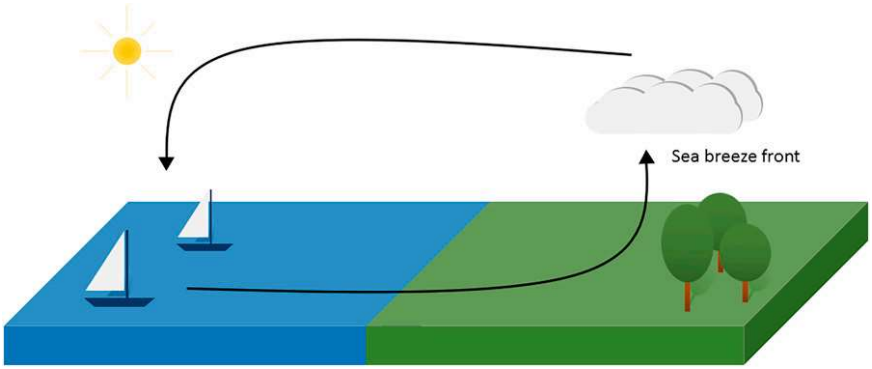

FIG. 1. Illustration of the sea-breeze circulation in the ideal case with quiescent synoptic conditions. The arrows indicate the direction of the circulation.

Thus, the sea breeze can be masked (see e.g., Sills et al. 2011) by the synoptic conditions, and no full circulation with return flow aloft occurs. In this study, we limit ourselves to only classifying the flow as a sea breeze if the winds are fully or partly opposing, comparing the 10-m wind direction with wind directions higher up in the boundary layer (see section 2a for further details).

Several attempts to forecast and characterize the sea breeze have been made, most relating the strength of the sea breeze to the observed temperature differences between land and sea, see e.g., Biggs and Graves (1962) who used dimensional analysis to create a lake breeze index based on the temperature difference and the surface wind speed. Following this work, Lyons (1972) used the geostrophic wind instead of the surface wind and Porson et al. (2007) performed nonlinear dimensional scaling using the surface heat flux instead of the temperature difference as one of the key variables. Frysinger et al. (2003) applied statistical methods to predict the sea breeze for Charleston, South Carolina, and Svensson et al. (2019) identified the sea breeze over the Baltic Sea in model data based on the temperature difference, the presence of a low-level jet, and by using a comparison with a "neutral wind model." Further, sea-breeze days have been categorized as days with sudden drops in inland temperature and a corresponding rise in relative humidity by, e.g., Physick and Byron-Scott (1977). Several studies have imposed criteria on the conditions of the winds on specific pressure surfaces, e.g., the 700-hPa level (Borne et al. 1998). For an overview of different filtering methods to identify the sea breeze, we refer to Steele et al. (2015). See also Crosman and Horel (2010) for a review of numerical studies on the sea breeze. Recently, machine learning methods have been applied to detect sea-breeze circulations from surface observations, see e.g., Sokolov et al. (2020), Roy et al. (2022) and Bedoya-Valestt et al. (2022). Using remote sensing techniques, ongoing sea-breeze circulations can often be recognized by the appearance of a sea-breeze front, and the characteristic band of cumulus or cumulonimbus clouds can be identified in satellite and radar images, either by inspection or using automated methods (see e.g., Wakimoto and Atkins 1994; Hadi et al. 2002; Planchon et al. 2006; Corpetti and Planchon 2011).

Since the end of the 2000s, the horizontal and vertical resolution of operational regional NWP (numerical weather prediction) models has become sufficiently high (only a few kilometers between grid points) to be able to resolve the sea- and land-breeze circulations. Although the circulations are driven by differences in temperature, in this study we propose a new measure to identify sea- and land-breeze circulations in NWP model output for any grid point close to the coast that is only based on the change of wind direction with height. Similar to a thunder probability index or an index to forecast the probability of icing on aircraft, a sea-breeze index (SBI) and land-breeze index (LBI) can present model output in a way which simplifies the work for the operational weather forecaster and assists in understanding and interpreting the weather situation. The indices could be used in mobile phone weather applications for coastal locations, to create sea- and land-breeze climatologies (see e.g., Furberg et al. 2002; Prtenjak and Grisogono 2007; Eager et al. 2008), or to characterize systematic biases in model output during the influence of sea or land breeze (see Banta et al. 2020, for a discussion on these matters). The method can also be directly applied to observations of the vertical profile by the wind in the coastal zone, e.g., performed through radio soundings or long-range lidar measurements. Further, implications for air quality (e.g., Kambezidis et al. 1998; Talbot et al. 2007; Wentworth et al. 2015) and offshore wind energy production (Steele et al. 2015; Xia et al. 2022) during days with and without sea breeze could be explored.

In this study, a straightforward method to identify sea- and land-breeze circulations in mesoscale resolving NWP model output based only on the turning of the wind in the column above a grid point is presented. In section 2, the general definition of the proposed SBI and LBI is presented, followed by a description of the NWP model HIRLAM–ALADIN Research on Mesoscale Operational NWP in Euromed (HARMONIE) Applications of Research to Operations at Mesoscale (AROME) that was used in the study. We will demonstrate that, with these new indices for the land and sea breeze, the occurrence of these circulations can be studied for different synoptic situations. To this end, we will use an objective classification method by Jenkinson and Collison (1977). This classification has

previously been utilized for many different applications. On the subject of winds in the coastal zone, we refer to Steele et al. (2015) for a study of sea breezes along the southern coast lines of the North Sea. Further, we also refer to Kalverla et al. (2019) for a study on the occurrence of anomalous wind events over the North Sea. In section 3, the results for two case studies and 5-yr summarizing statistics for seven coastal locations in southern Sweden are presented. A discussion and several suggestions for further development of the method is given in section 4, followed by a summary and some conclusions in section 5.

2. Method and materials

a. *Definition of the SBI and LBI*

The general idea behind the proposed method to calculate the SBI and LBI is to present a method that is straightforward to apply to vertical profiles and that captures the characteristics of the opposing winds at lower and upper levels in the coastal zone during the occurrence of sea or land breeze. The method is based only on the wind direction relativethe coastline using three angles, see the illustration in Fig. 2: the angle perpendicular to the coastline (ϕ), the wind direction of the 10-m wind (α), and the wind direction of an upper-level wind (β) (see section 2c for details). The angle ϕ was defined to be the same as the wind direction for a wind directed from sea toward land perpendicular to the coast, i.e., for the west coast of a land area, $\phi = 270°$.

To calculate the SBI or LBI for a grid point at the coast, the following three criteria have to be met:

1) SBI: α is within $\pm 90°$ from ϕ (i.e., the 10-m wind is at least partly directed from the sea toward land)
   LBI: α is within $\pm 90°$ from $\phi + 180°$
2) SBI: β is within $\pm 90°$ from $\phi + 180°$ (i.e., the wind at the upper level is at least partly directed from land toward the sea).
   LBI: β is within $\pm 90°$ from ϕ
3) SBI and LBI: β is within $\pm 90°$ from $\alpha + 180°$ (i.e., the upper wind is at least partly in the opposite direction as the 10-m wind, see the sector marked in Fig. 2)

If all criteria were met, the SBI was calculated as

$$\mathrm{SBI} = \cos(\alpha - \phi) \times \cos(\alpha + 180° - \beta), \quad (1)$$

or, similarly, the LBI was calculated as

$$\mathrm{LBI} = -1 \times \cos(\alpha - \phi) \times \cos(\alpha + 180^{\circ} - \beta). \quad (2)$$

As such, it is clear that both the SBI and the LBI will take values between 0 and 1. The highest values of the SBI (LBI) will occur if the 10-m wind is perpendicular to the coast and directed toward land (sea) with fully opposing winds at the upper level. The lowest values of the SBI and the LBI will both occur in cases when either the 10-m wind is close to being parallel to the coastline (although with some component directed over the coast) and/or if the upper wind is close to being perpendicular to the 10-m wind.

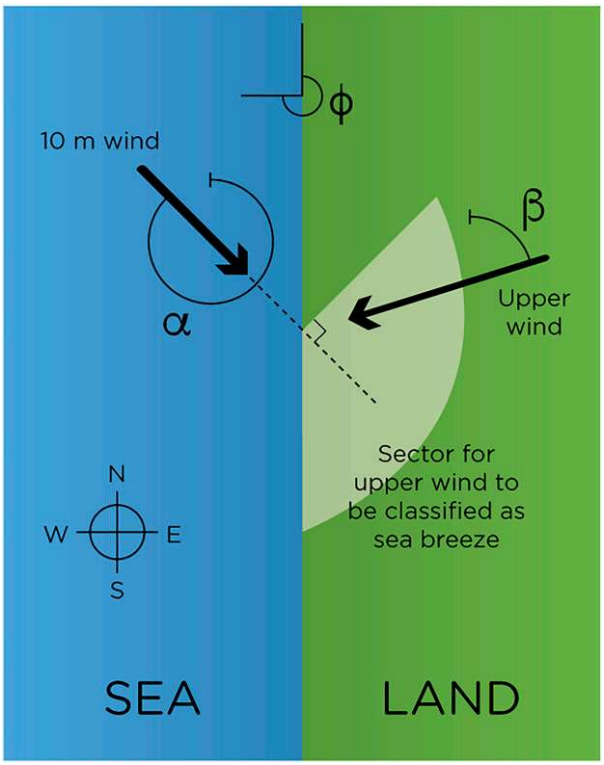

FIG. 2. Illustration of the definition of the three angles ϕ, α, and β that are required to calculate the SBI and LBI. In this example, a weak sea-breeze circulation is occurring as the upper wind is far from fully opposing the 10-m wind.

The SBI and LBI can be thought of as the degree of opposing winds perpendicular to the coast. Although we use the notation SBI and LBI and often refer to the corresponding phenomena as sea breeze or land breeze, respectively, we want to stress that the shift in wind direction in the vertical profile could occur due to other local, mesoscale or synoptic features, such as e.g., thunderstorms, capping inversions or frontal passages. As mentioned in section 1, we only consider cases of sea and land breezes when the return flow is not masked by a superimposed synoptic scale wind. Also cases when the synoptic wind prevents the circulation from moving onshore or when the synoptic wind deforms the circulation are omitted. Note that no criteria on the season or the time of day when the sea and land breeze can occur were imposed. Also, note that by definition the sea and the land breeze cannot occur simultaneously and at any given point in time and space, either SBI or LBI (or no value) can be calculated, due to the postulated criteria.

b. *HARMONIE-AROME*

To identify the sea and land breezes in NWP model output, a model of sufficiently high resolution to resolve mesoscale phenomena in the coastal zone is needed. In this study, we choose to use HARMONIE-AROME, a convection permitting NWP model with 2.5-km horizontal resolution, 65 terrain-following hybrid sigma vertical levels and a

75-s time step (Bengtsson et al. 2017; Vignes 2021). The model domain (approximately 53°–73°N and 5°W–35°E) covers Scandinavia and the Baltic states as well as the Nordic seas and is used for operational weather forecasting by meteorological institutes in Sweden, Denmark, Norway, Finland, and Estonia among others. On the boundaries, HARMONIE-AROME is driven by the global IFS (Integrated Forecasting System) model from the ECMWF (European Centre for Medium-Range Weather Forecasts). HARMONIE-AROME is a 30-member probabilistic system, where the control member is run with full forecast length every 3 h (0000, 0300, 0600, … UTC). The maximum length of the operational forecasts is 66 h with hourly time steps stored in the output. In this study, only forecasts from the control member issued at 0000 UTC and with forecast lengths of 0–23 h were used.

c. *Calculating the SBI and LBI from HARMONIE-AROME output*

To calculate the SBI and the LBI for a grid point in the coastal zone using HARMONIE-AROME data, the 10-m wind components were obtained together with wind components from model levels 62–38. The angle ϕ was manually defined for the selected sites in this study.

To identify the return flow of the sea breeze, wind directions at model levels 51–38 were used, roughly corresponding to heights between 500 and 2000 m above the surface (more specifically, 542–1953 m in the standard atmosphere). The wind directions at all these levels were checked independently to see if they fulfilled the criteria presented in section 2a, and if so, the SBI was calculated for that level. The maximum SBI among all levels was kept and considered to be the final SBI for that site and time step. As the land-breeze circulation typically is shallower, the LBI was calculated in a similar way but only using model levels in the range 46–62 to identify the upper level flow, roughly corresponding to heights of 100–900 m above the surface (89–927 m in the standard atmosphere).

d. *Synoptic classification*

To categorize the synoptic conditions over the southern part of Sweden the objective Jenkinson and Collison (1977) method was applied to find the Lamb weather type (LWT) for each time step in the analysis (Lamb 1972; Jones et al. 2012; Fernández-Granja et al. 2023). The method makes use of sea level pressure at 16 grid points placed as marked in Fig. 3. With the focus area centered at 57°N, 15°E the HARMONIE-AROME domain does not cover the location of all 16 grid points, and thus reanalysis data from the fifth-generation ECMWF reanalysis ERA5 (Hersbach et al. 2020) was used instead. ERA5 is a global, state-of-the-art reanalysis with a horizontal resolution of 0.25° × 0.25° and hourly data.

Based on the variation in surface air pressure between the 16 grid points a synoptic vorticity and a representative wind (speed and direction) were calculated for the focus area. The synoptic situation was then classified as one of the 27 Lamb weather types:

- purely anticyclonic (A)
- purely cyclonic (C)

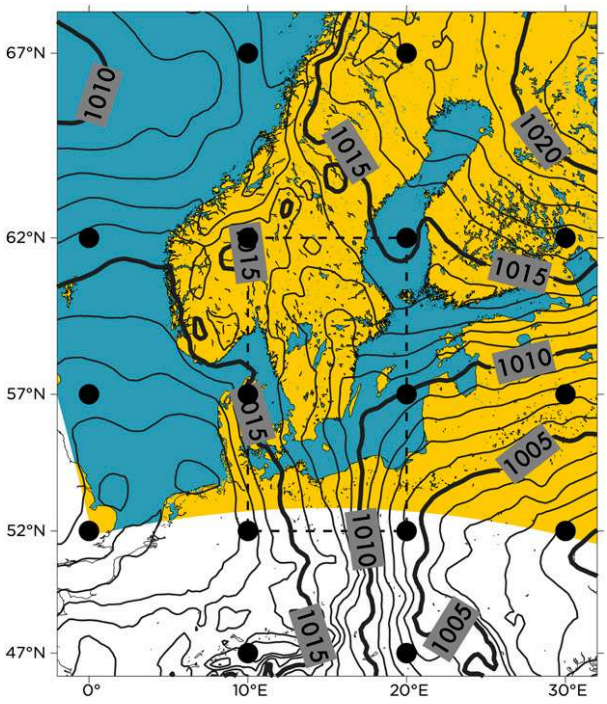

FIG. 3. Map of Scandinavia showing the location of the 16 grid points (marked in black) used for the LWT classification by the Jenkinson and Collison (1977) and the focus area where the classification is valid (within the dashed line). The land (sea) mask from HARMONIE-AROME is plotted in yellow (blue), indicating the southern boundary of the model domain. The isobars show an example of the ERA5 normalized sea level pressure field (labels in hPa) at 1200 UTC 18 Jul 2018 (used for case study 2), for which the LWT was classified as type N and the synoptic wind speed as moderate in the focus area.

- eight classes of directional flow (N, NE, E, …)
- 16 classes of hybrid flow that represent anticyclonic or cyclonic flow with a component of directional flow (such as AN, ANE, …, CN, CNE, …)
- weak flow (U)

Further, the synoptic wind speed was divided into four categories of equal relative occurrence: weak, moderate, strong, and very strong.

e. *Study design: Case studies and 5-yr overview*

As a proof-of-concept and to test the proposed methodology to identify sea and land breezes using HARMONIE-AROME model output, two case studies were performed. In the first case study (25 July 2018), a sea-breeze circulation was clearly occurring along a great part of the coast in southern Sweden, see the satellite image in Fig. 4a. Three transects were drawn to study the sea-breeze circulation, as marked in Fig. 4b: one transect from south to north (transect A–B) and two transects from west to east (transects B–C and D–E). Further, seven coastal sites were selected, and their angle ϕ was manually determined, also marked in Fig. 4b. As seen in Fig. 4b, the sites are spread out on the western, southern, and

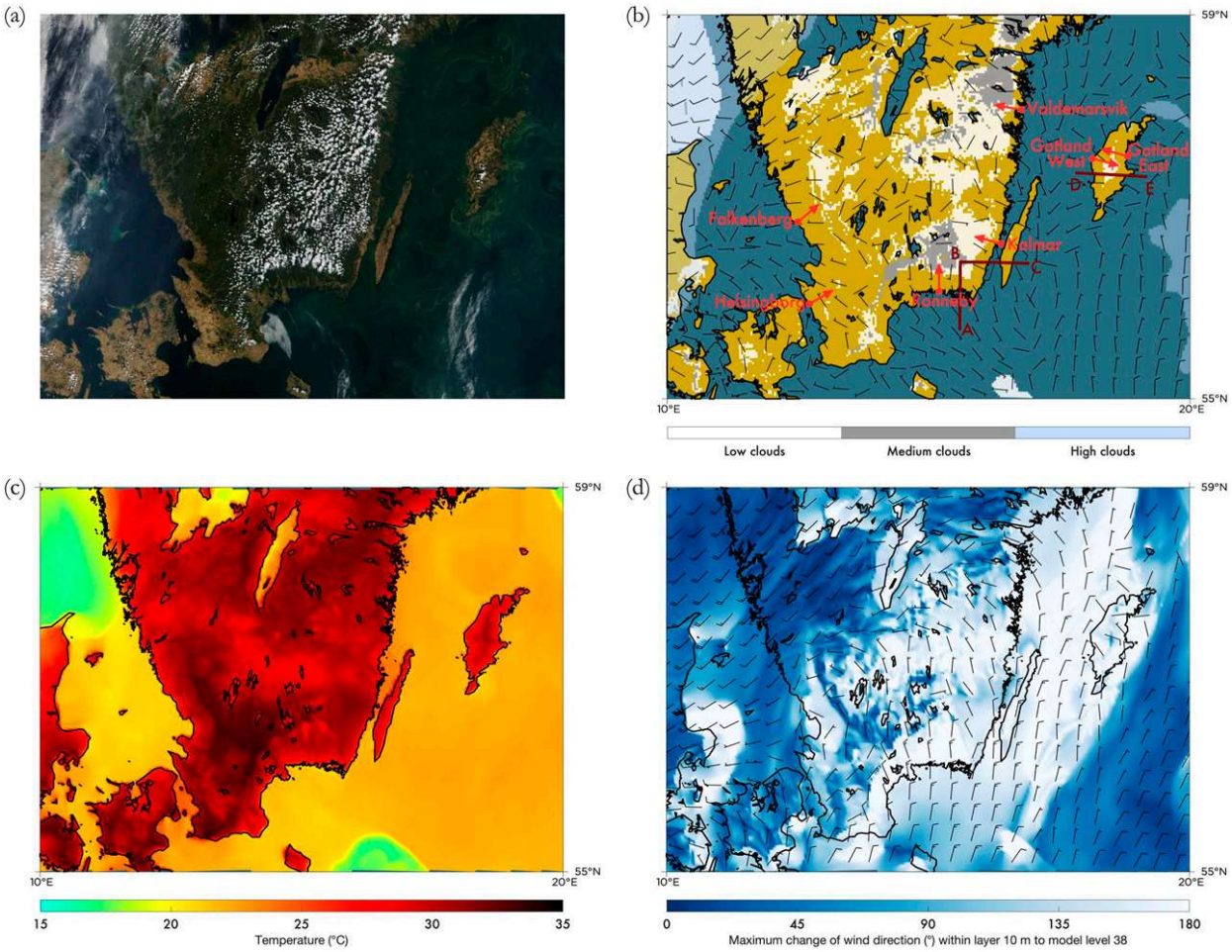

FIG. 4. (a) True color satellite image with corrected reflectance from the MODIS instrument on the *Terra* satellite, showing southern Sweden at 1200 UTC (1300 LST) 25 Jul 2018. (b) The HARMONIE-AROME forecast for the same date and time, visualizing the amount of clouds (low, medium, and high clouds) and with wind barbs showing the speed and direction of the 10-m wind (wind direction shafts are directed upwind from the grid points with long barbs representing wind speeds of 10 kt and half-barbs representing wind speeds of 5 kt placed at the end of the shaft; 1 kt $\approx$ 0.51 m s^{-1}). Three transects (A–B, B–C, and D–E) are marked on the map, together with the location of the seven coastal sites used in the study. The angle ϕ is indicated by the red arrow for each site. (c) The 2-m temperature and (d) the maximum change of wind direction (colored field) comparing the 10-m wind direction with wind directions from model levels 65–38 is visualized (not considering if the turning is clockwise or counterclockwise), together with wind barbs showing the wind speed and direction at model level 38 (approximately 2000 m above the surface). We acknowledge the use of satellite imagery from the Worldview Snapshots application (https://wvs.earthdata.nasa.gov), part of the Earth Observing System Data and Information System (EOSDIS).

eastern coasts and have a varying degree of complexity of the coastline, where Helsingborg and Kalmar represent the most complex as they are both located close to narrow straits.

The second case study was performed for 18 July 2018 when a cold front passed over the southern parts of Sweden. This case study demonstrates potential shortcomings of the proposed index and how the results should be interpreted given different governing synoptic conditions. As for the first case study, the change of wind speed and direction throughout the day was plotted for the same set of coastal sites in southern Sweden.

A 5-yr overview of annual occurrence of sea and land breezes at the seven sites was also studied, together with the seasonal variation and the diurnal cycle, using archived HARMONIE-AROME data between 1 January 2017 and 31 December 2021. The main limitation for a longer time series was that no forecasts were archived pre-November 2016. The time period January 2017–December 2021 was selected in order to get full years, without bias to any a specific season. For both the case studies and the five year statistics, deterministic forecasts issued at 0000 UTC were used (see also section 2b), analyzing forecasts with a lead time of 0–23 h.

3. Results

a. *Case study 1: A textbook example of sea-breeze circulation*

The summer of 2018 was dominated by a sequence of blocking high pressure systems and unusually high temperatures

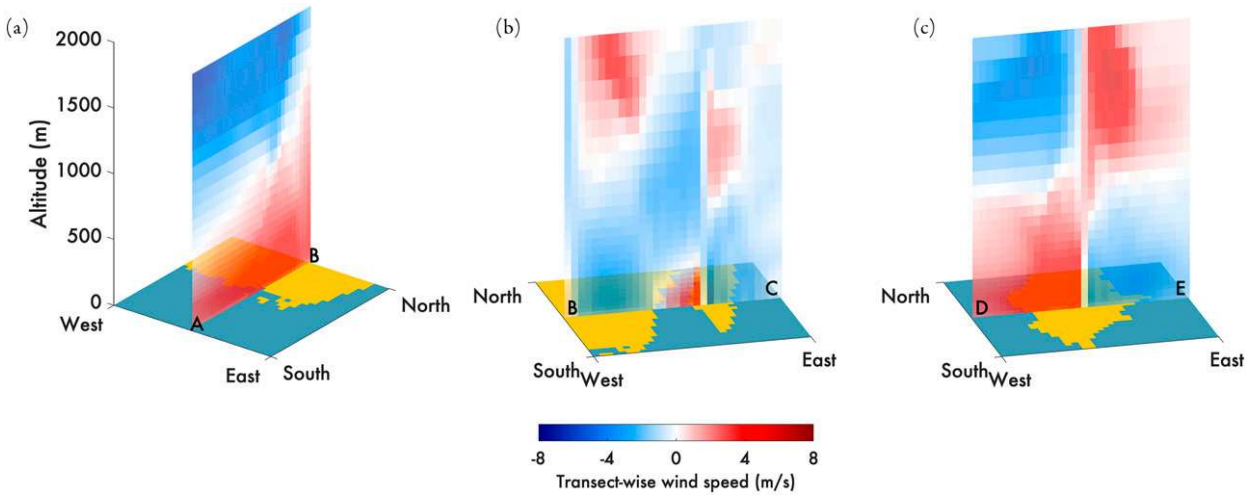

FIG. 5. Cross section of wind speed following the transects (a) A–B, (b) B–C, and (c) D–E as marked in Fig. 4b. The vertical coordinate is given as the altitude in the standard atmosphere.

over northern Europe (e.g., Wilcke et al. 2020; Yiou et al. 2020). At the time of the case study, 25 July 2018, a heat wave affected Scandinavia with temperatures reaching up to 30°–35°C in a great part of southern Sweden (see Fig. 4c) and a high pressure system of approximately 1015–1020 hPa caused weak synoptic flow; see the wind barbs in Fig. 4d. The synoptic situation was classified as type U (see section 2d) for all hours throughout the day. The contrast between the temperature over the sea and over the lakes compared to over land was pronounced with sharp gradients in the coastal zones. All in all, the conditions were very favorable for sea-breeze formation. In the satellite image from *Terra* using the Moderate Resolution Imaging Spectroradiometer (MODIS) instrument, Fig. 4a, it can be seen that sea-breeze circulations were occurring along a great part of the east and south coasts in southern Sweden as the sea-breeze front pushed the formation of convective clouds inland; compare with the illustration in Fig. 1. Also, cloud formation along the midline of Gotland (the largest island in the Baltic Sea) suggests that possibly two sea-breeze circulations, one on the east coast and one on the west coast of the island, could be present.

The HARMONIE-AROME forecast issued at 0000 UTC 25 July, valid at 1200 UTC, described the cloud conditions in a satisfying way, comparing the forecast map in Fig. 4b with the satellite image in Fig. 4a. The forecast captured the formation of convective clouds in both the southeastern part of mainland Sweden and on Gotland. The wind barbs in the forecast map show that in many places along the coast, the 10-m wind was directed partly from sea toward land and that wind speeds in general were weak to moderate, 0–5 m s^{-1} (0–10 kt).

HARMONIE-AROME also forecast a significant wind turning with height, as can be seen by comparing the wind direction at 10 m with wind directions on all forecast levels above, up to model level 38. The maximum possible wind shift (180°) was predicted in the southeastern parts of Sweden, over eastern Jutland (in the westernmost part of the map) and over a great part of the Baltic Sea, matching the areas where sea-breeze circulation could be expected from the satellite image. Wind shifts greater than 90° were also predicted over Lake Vänern and Lake Vättern (the two largest lakes in the map) but the clouds seen here are less likely to be forced by sea-breeze circulation due to the 10-m wind direction in the area, see Fig. 4b. Also, locally at the Swedish west coast, the change of wind direction with height was pronounced, and what could be interpreted as a sea-breeze front was indicated by the cloud cover in the HARMONIE-AROME output (Fig. 4b). However, in reality the conditions were slightly drier than predicted and no clouds were visible in this region in the satellite image, at least not for the chosen point in time.

Vertical cross sections using data from model levels 65–38 of the transectwise wind speed for the three transects A–B, B–C, and D–E (see Fig. 4b) are presented in Fig. 5. Every transect consists of 33 columns of grid points, corresponding to a distance of 80 km from the start to the end of the transect. The south–north transect A–B in Fig. 5a displays a pure sea-breeze circulation with southerly winds directed from the sea toward land at low levels and with a reversed flow (northerly winds) higher up. Note that the transition from a southerly to a northerly wind component, marked as the white band in the figure, occurred higher up over land than over water, indicating the difference in the height of the boundary layer (cf. also to Feliks 1993). The transect B–C in Fig. 5b covers a complex coastline as it first passes over mainland Sweden, then over a narrow strait (five grid points), over the narrow island Öland (six grid points) and finally out over the Baltic Sea. Close to the surface, the winds were mostly easterly over mainland Sweden, switched to more westerly winds over the strait and then switched back to easterly winds over Öland and the Baltic Sea, indicating convergence of the flow and a possible sea-breeze circulation over Öland. For mainland Sweden, a sea-breeze front is visible both in the satellite image, Fig. 4a, and in the forecast map, Fig. 4b, but the west–east circulation in this area is not so pronounced. Note that the same grid point, B, was used for both transect A–B (Fig. 5a) and

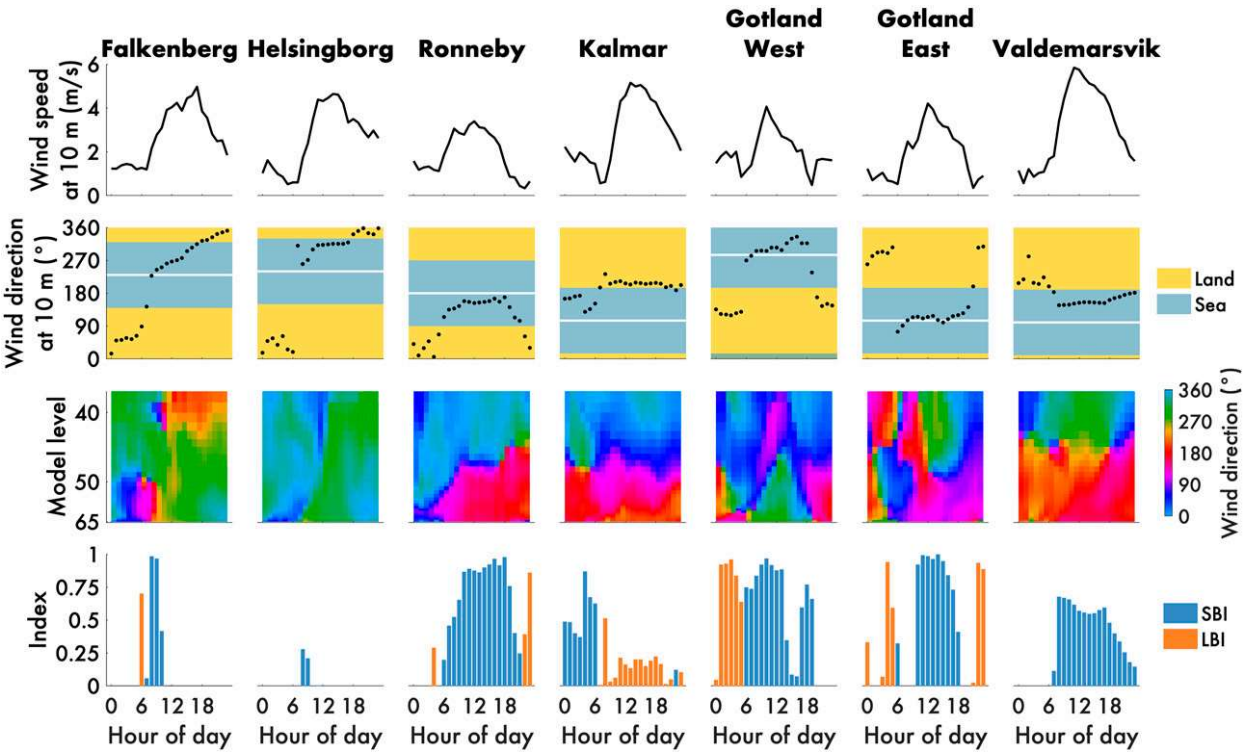

FIG. 6. Forecast temporal evolution of (first row) the 10-m wind speed, (second row) the 10-m wind direction, (third row) vertical profiles of wind direction, and (fourth row) SBI and LBI for the seven selected sites during 25 Jul 2018. Data are from the HARMONIE-AROME forecast issued at 0000 UTC with a forecast length of 0–23 h. The spacing of the model levels for the vertical profiles (third row) is based on the height of the model levels in the standard atmosphere. The background coloring on the second row marks if the 10-m wind is directed from the land sector or the sea sector and the solid white line marks the angle ϕ for each site.

transect B–C (Fig. 5b), and thus it is clear that the south–north sea-breeze circulation was dominating at the site.

The transect D–E in Fig. 5c passes over Gotland but with both start and finish in the Baltic Sea. As there was convergence over the island at low levels but divergence higher up, the vertical cross-section suggests that a double sea-breeze circulation was occurring, one on the west coast and one on the east coast of the island. Both these circulations contributed to the convection over Gotland and the formation of the cumulus clouds seen both in the satellite image and in the forecast map, Figs. 4a and 4b.

The forecast time evolution of 10-m wind speed and direction, as well as the change in wind direction with height throughout the day (0–23-h forecast length) for the seven selected sites (marked in Fig. 4b) is plotted in Fig. 6. In the figure, also the SBI and LBI for every hour is presented. Starting with the wind speed, it is clear that all sites exhibited an increase in the wind speed during the morning and then decreasing winds in the afternoon/evening. For most sites, there was also a clockwise rotation of the wind as the wind increased, related to the Coriolis effect. This turning was, however, not seen for Kalmar, where channeling of the wind in a south–north direction along the strait was the dominant factor. Studying the vertical profile of wind direction and how it changed throughout the day, it is clear that major wind shifts of over 90°, and even up to 180°, can occur over short vertical distances and that only Helsingborg displayed a rather constant wind direction with height; compare also with Fig. 4d.

The SBI values suggest that pronounced sea-breeze circulations were occurring in Ronneby, on both sides of Gotland and in Valdemarsvik (cf. with transect A–B close to Ronneby in Fig. 5a and transect D–E over Gotland in Fig. 5c). For these sites there was an onset of the sea breeze during the morning hours and the circulation lasted until the evening. Also in Falkenberg and in Helsingborg, short-lived sea breeze circulations were identified in the morning.

As indicated by the transect B–C in Fig. 5b, the flow situation over Kalmar was more complex. For the selected grid point, the 10-m wind was from south-southwest during most of the day (see Fig. 6), implying that there was a wind component directed from land toward the sea, although almost parallel to the coastline. The channeling effect became less pronounced with increased vertical distance from the surface, since the winds turned via easterly winds toward the geostrophic wind which was mostly northerly in the area (Fig. 4d). The circulation was classified as a land breeze, although with rather low values of the LBI. For both sides of Gotland as well as in Ronneby, land-breeze circulations were occurring before and/or after the sea breeze. Note that for the site Gotland West, no land breeze was detected in the evening, as the upper wind

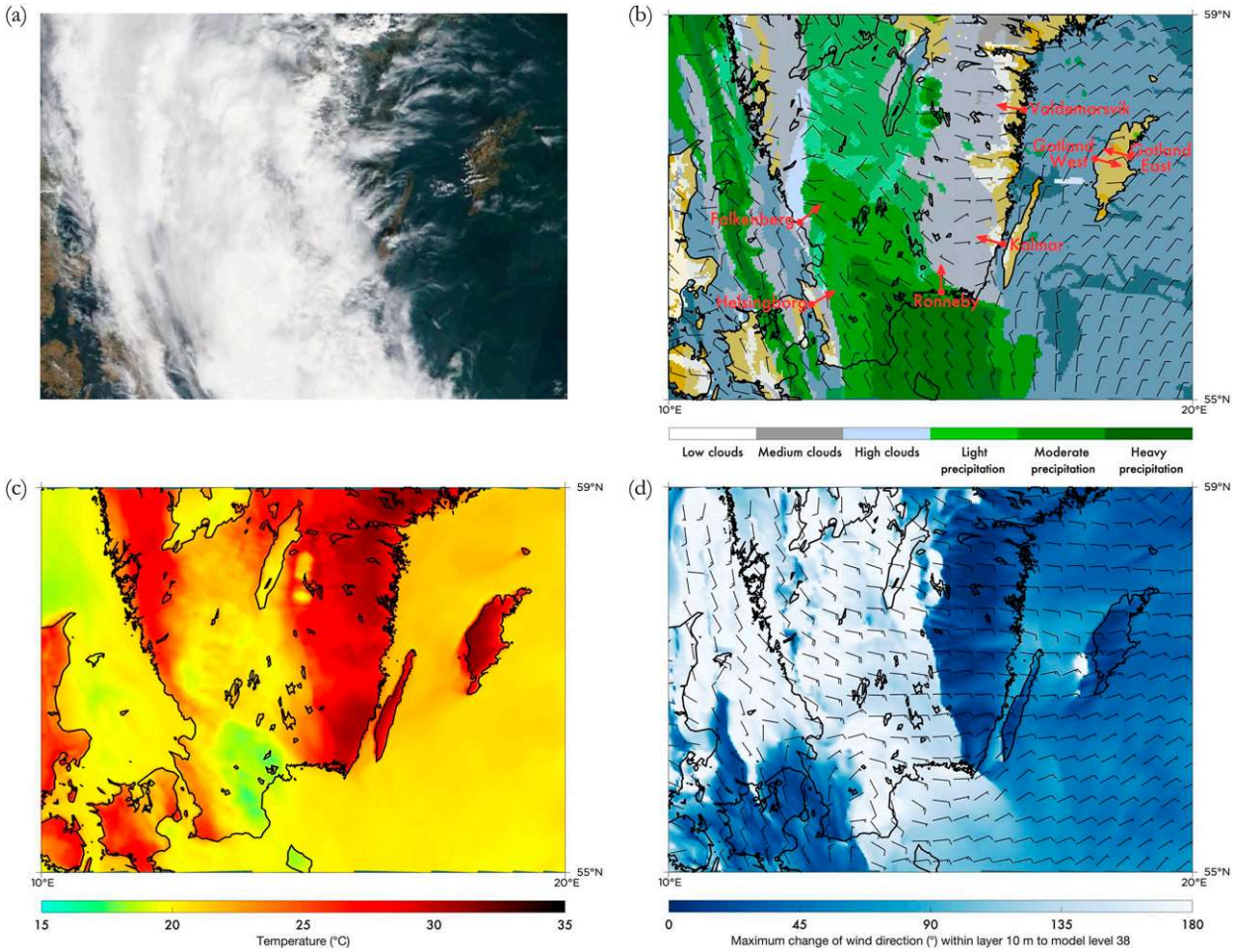

FIG. 7. (a) The satellite image of southern Sweden at 1200 UTC (1300 LST) 18 Jul 2018; and (b) the HARMONIE-AROME forecasts for the same date and time, visualizing the amount of clouds (low, medium, and high clouds) and the intensity of precipitation. (c) The 2-m temperature and (d) the maximum turning of the wind comparing the 10-m wind direction with wind directions from model levels 65–38 is visualized. More details about the panels can be found in the caption for Fig. 4. We acknowledge the use of satellite imagery from the Worldview Snapshots application (https://wvs.earthdata.nasa.gov), part of the Earth Observing System Data and Information System (EOSDIS).

direction (β) at levels 46–62 was not within $\pm 90°$ from $\alpha + 180°$ (see details in method description, sections 2a and 2c).

b. *Case study 2: Passage of a cold front*

On 18 July 2018 a cold front passed over southern Sweden, bringing rain and locally lower temperatures, see Figs. 7a–c. As for case study 1, the land–sea temperature gradient was pronounced and the winds were in general weak, but the front prevented the formation of the mesoscale sea-breeze circulation. However, the cold front was associated with a major turning of the wind direction with height, up to 135°–180° in a great part of the study area (Fig. 7d). The synoptic wind was classified as moderate all day and the LWT as type NE until 0900 UTC and then as type N for the rest of the day. In Fig. 3 a visualization of the sea level pressure field at 1200 UTC is presented.

The temporal evolution of wind speed and wind direction at 10 m, the wind profile and the SBI and LBI values are plotted in Fig. 8 for the same seven sites as presented in case study 1. The passage of the cold front is clearly visible for Falkenberg with a distinct peak in the 10 m wind speed and a simultaneous change in wind direction. As can be seen in the vertical profile of wind direction for Falkenberg, the wind shift started at the lower levels and propagated upward over time. This vertical slant in wind direction resulted in values of the SBI well exceeding 0.5. For Helsingborg, the change in the 10-m wind direction was smaller and consequently also the turning of the wind with height. As the winds were almost parallel to the coastline, the values for the SBI were small. For Ronneby, the HARMONIE-AROME forecast showed a quick change in wind direction in the morning hours, also resulting in a short period with SBI. The other sites were experiencing less of the direct effects of the cold front, and

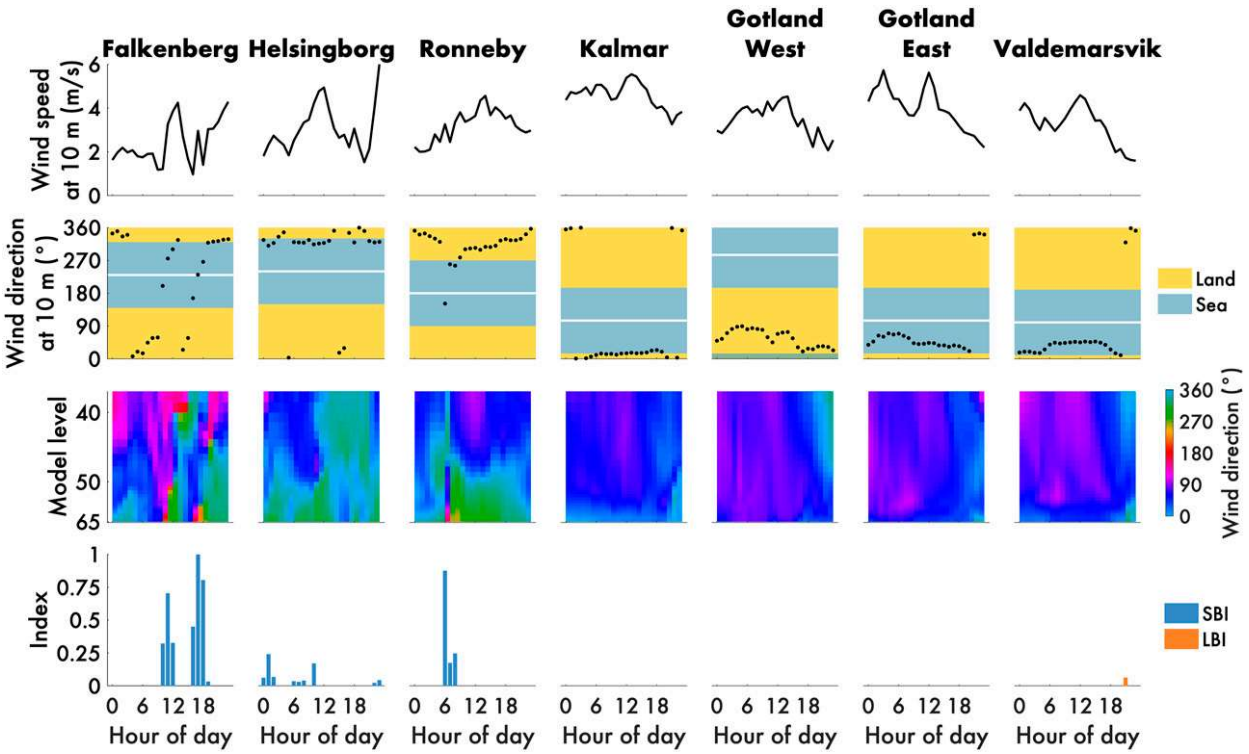

FIG. 8. Forecast temporal evolution of (first row) the 10-m wind speed, (second row) the 10-m wind direction, (third row) vertical profiles of wind direction, and (fourth row) SBI and LBI for the seven selected sites during 18 Jul 2018. More details about data presented in the panels can be found in the caption for Fig. 6.

only for Valdemarsvik there was a (low value) LBI in the late evening.

c. *Five-year statistics*

The 5-yr statistics of SBI and LBI occurrence for the seven selected coastal locations in southern Sweden are presented in Fig. 9. No thresholds were used for SBI or LBI, i.e., all occasions with even the slightest sea- or land-breeze circulation as classified by the method in section 2c were included in the results. Note that, as only five years of data were analyzed, the results indicate the performance of the indices, but not the climatological behavior. Also, keep in mind that the indices signal opposing winds with height. However, the indices are not a sufficient condition for land breeze and sea breeze, as shown in the second case study.

On average, SBI and LBI each appear approximately 5% of all the hours in a year, for all sites and all years analyzed. Although some annual variation is expected due to differences in governing synoptic conditions, there were no major differences between the different years for a given site, except that in 2018 when the SBI was slightly more frequent than in other years. This peak was probably related to the dominating quiescent synoptic conditions and extended heat wave in that year (Wilcke et al. 2020; Yiou et al. 2020), leading to unusually large land–sea temperature differences and thus good preconditions for sea-breeze formation. It can also be seen that sites on the east coast (Kalmar, Gotland East, and Valdemarsvik) experienced SBI more often, and LBI less often, than sites on the west coast, explained by the fact that southwesterly winds are the predominant climatological geostrophic wind direction over southern Sweden. The seasonality plots show that the SBI had a pronounced seasonal cycle being more frequent in the period April–September than during the other half of the year, as expected for this study area. For most sites, May, June, and July were the months where SBI (>0) occurred most frequently, up to 10%–20% of the hours in the month. However, for individual years the relative frequency of SBI could reach up to 30%–40% for these months (not shown). As the seasonal pattern is clear for the SBI, the same is not true for LBI which seemed to be more uniformly distributed throughout the months of the year.

Diurnal cycles showed that SBI was more frequent during the day, with a peak at noon, and LBI being more frequent during the night, with a peak in the late night/early morning. This indicates that the indices to a large extent performed as expected for the studied sites. Peak frequency values indicate that approximately 10% of days will exhibit SBI or LBI at the respective peak hour. Applying a threshold of 0.25 or 0.5 for SBI and LBI did not significantly alter the pattern of the diurnal relative occurrence other than, of course, decreasing the values.

The site that differed most from the others, both in terms of annual relative occurrence and in the diurnal cycle, was Kalmar. Again, the alignment of the 10-m winds along the

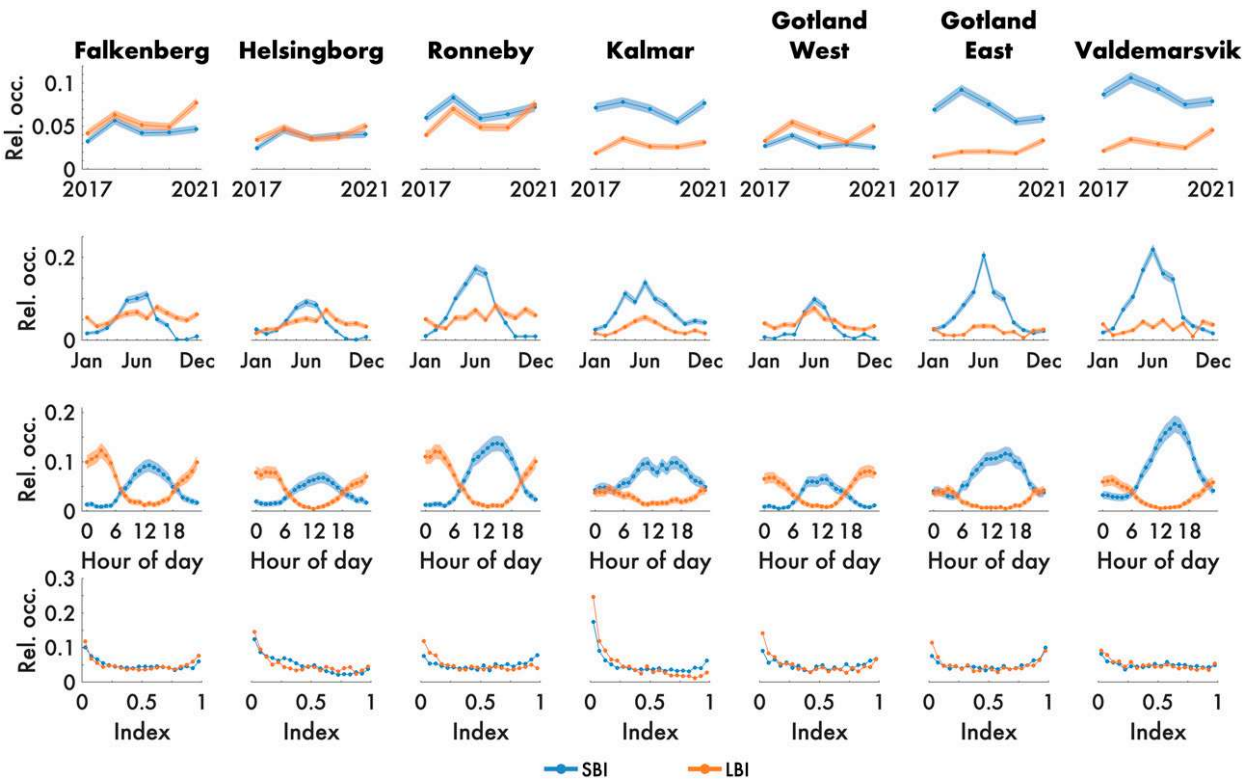

FIG. 9. Annual relative occurrence of (first row) SBI and LBI 2017–21, (second row) seasonal cycle, and (third row) diurnal cycle. Times are in UTC (LST − 1 h). (fourth row) The distributions of SBI and LBI are presented using a bin size of 0.05. Shaded areas around the lines (top three rows) mark the 95% confidence intervals of the relative occurrence.

strait with weak flow on or off the coast was the reason for these patterns. This can also be seen in the distributions of SBI and LBI where there was a larger share of very small indices (indicating weak circulations or winds being close to parallel to the coast) compared to other sites. It is likely that for this site there was less correlation between the 10-m wind (channeled) and the upper (geostrophic) wind than for other sites where the distributions of SBI and LBI were more uniform. Interestingly, for some of the sites (e.g., Falkenberg, Ronneby and the two sites on Gotland), there seemed to be a tendency toward a slight increase of the relative occurrence of the SBI (for Gotland also the LBI) close to the index value 1, implying that when the 10-m wind was close to being perpendicular to the coast and directed from the sea toward land, it was actually more likely that the upper wind at some model level would be in the complete opposite direction (or close to that) than in some other direction.

By applying the Jenkinson and Collison method to the ERA5 surface pressure field the synoptic conditions were classified and associated with a corresponding LWT and synoptic wind speed category for every hour in the 5-yr period analyzed. Pure anticyclonic (A) and pure cyclonic (C) conditions were the most common LWTs, appearing 15.7% and 13.0% of the time, respectively, as shown in Fig. 10. The dominating wind direction in the study area is from southwest to northwest and LWTs for these classes are the most commonly occurring, both for the pure directional flow and for hybrid flow. Quiescent synoptic conditions (type U) occurred approximately 4% of the time in total. The seasonal variation of relative occurrence differs between the LWTs. For example, type U occurs 10% of the time in summer (June–August) but only 1% of the time in winter (December–February), not shown.

In Fig. 10a, also the relative occurrence of SBI given the LWT is presented for the seven selected coastal locations in southern Sweden. For all sites, except Gotland West, the LWT with the highest relative occurrence of SBI is type U. Given this LWT, SBI (>0) occurs approximately 15%–30% of the time. Note that all hours of the year (day and night) are included in the analysis. For Gotland West, type ASE coincides with the highest relative occurrence of SBI.

In general, SBI occurred more often in anticyclonic (A) than in cyclonic (C) conditions, also taking hybrid flow (AN, ANE, … and CN, CNE, …) into account. Further on, sites located on the east coast (Kalmar, Gotland East and Valdemarsvik) display SBI > 0 during synoptic conditions with a dominant wind direction from southeast or south. On the other hand, sites on the west coast (Falkenberg and Helsingborg) show SBI > 0 most commonly when the synoptic flow is directed from the southeast. Also, for Ronneby, located on the south coast, LWTs indicating flow from north or northeast are beneficial for SBI, apart from types U and A. The lower relative occurrence of SBI for LWTs with wind directions

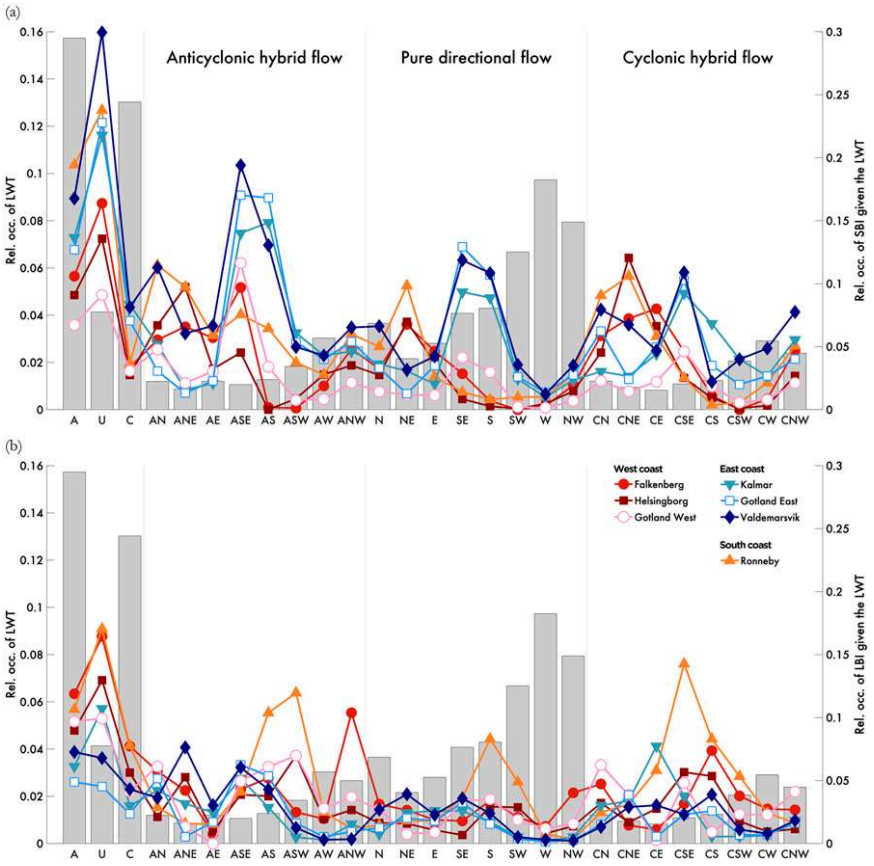

FIG. 10. Relative occurrence of the 27 different LWTs for the focus area (marked in Fig. 3) during the years 2017–21 (gray bars). The lines show the relative occurrence of (a) SBI and (b) LBI given the LWT for the seven selected coastal sites.

from southwest to northwest is probably related to the stronger winds generally associated with these LWTs. The relative occurrence of SBI given the different synoptic wind speed categories (all by definition occurring 25% of the time) is presented in Fig. 11. For all sites, SBI > 0 is most frequently occurring in weak synoptic forcing (in general 10%–20% of the time) and decreases in frequency as the wind speed increases. Although situations with strong or very strong synoptic wind speed are less favorable preconditions for formation of mesoscale circulations, it should be noted that the proposed method is able to identify SBI also in these conditions. Additionally, despite the lower relative occurrence of SBI

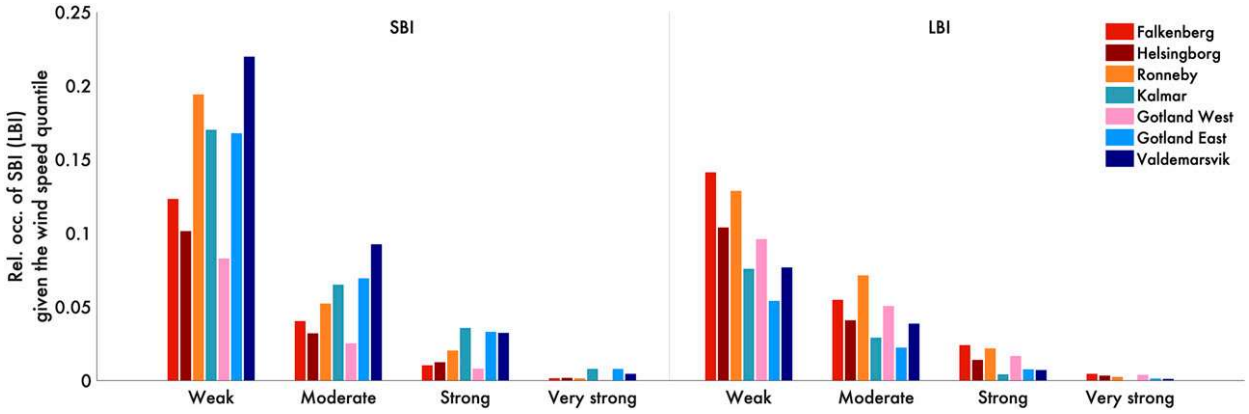

FIG. 11. Relative occurrence of (left) SBI and (right) LBI given the synoptic wind speed quantile for the seven selected coastal sites.

during LWTs with wind directions from southwest to northwest, they still have a significant contribution to the overall occurrence of SBI as they are among the most frequently occurring LWTs.

Results for the relative occurrence of LBI given the different LWTs are presented in Fig. 10b and given different synoptic wind speed categories in Fig. 11. Similar to the results for the SBI, the LBI is most frequently occurring in weak or moderate synoptic forcing, i.e., type U or type A. As for SBI > 0 the relative occurrence of LBI > 0 during pure flow direction from the sector southwest to northwest is less frequent compared to other wind directions. This is most clearly seen for the sites at the east coast. Generally, the correlation between LBI and the LWTs was less clear for LBI compared to SBI, but in terms of synoptic wind speed the pattern is similar.

4. Discussion and outlook for future work

The proposed method to identify sea and land breezes in operational NWP model output presented in section 2 showed promising results both for case study 1 (section 3a) and for the 5-yr overview for coastal sites in southern Sweden (section 3c), capturing the expected diurnal cycles and seasonalities well (Figs. 6 and 9). One of the main drawbacks of the method is the performance in areas with a high degree of coastline complexity; see the example of SBI and LBI for Kalmar in Fig. 6. On the other hand, for Helsingborg the classification scheme performs well, despite the narrow strait between Sweden and Denmark. Also, certain weather situations are problematic for the classification scheme, e.g., during passages of cold fronts (case study 2). However, also in these conditions, the SBI and LBI can provide the operational weather forecaster with the information that there is a strong change in wind direction with height, and the direction of the circulation—although it is neither a sea breeze nor a land breeze occurring. In the following discussion, several ideas to further refine the classification scheme are presented.

The most convenient way to fine tune the methodology would be to restrict the occurrence of sea breezes and land breezes to specific months of the year, or specific hours of the day, based on a known climatology for the area where the method is implemented. Further, as both the sea and land breezes are events lasting multiple hours, temporal criteria could be imposed. In the current form, individual hours or very short events with sea or land breeze could be captured (see, e.g., the results for Helsingborg and Ronneby, in both case studies, Figs. 6 and 8). This could either be related to the fact that a sea- or land-breeze circulation actually was occurring (presumably in case study 1) or related to, e.g., a frontal passage or isolated convective cells with rapid changes in wind direction with height. Following the methodology of Steele et al. (2015), an additional criterion regarding the governing synoptic conditions could be added, e.g., not calculating the SBI or LBI if the LWT is classified as one of the cyclonic types. However, as we wanted to keep the SBI and LBI in their purest form in this study, to show both the strengths and weaknesses of the proposed method, implementation of these ideas was not carried out.

Validating the index is challenging, but could be done by comparing with results from other numerical methods (see e.g., Frysinger et al. 2003; Porson et al. 2007) or with results from remote sensing detection of coastal circulations (see e.g., Hadi et al. 2002; Planchon et al. 2006). The index could also be validated against a manual classification performed by an experienced meteorologist. Such a dataset, spanning five years for random stations globally, has been created by Bedoya-Valestt et al. (2022) but is yet to be released.

To minimize the problem of erroneously classified sea breezes or land breezes due to channeling of the wind in narrow straits, a stricter criterion on the allowed difference in wind direction between the 10-m wind (α) and the direction perpendicular to the coastline (ϕ) could be used. In this study, the angle ϕ was manually defined for the seven sites. For a full application along the entire coastline of a country, an automatic procedure would be needed. However, peninsulas and archipelagos where no dominant direction of the sea or land breeze can be easily defined (see Gustavsson et al. 1995) and coastlines with complex topography where katabatic winds are common (see Miao et al. 2003) will remain challenging for the method.

It is possible to extend the calculations of SBI and LBI both onshore and offshore as long as it is clear which is the dominating coastline, i.e., how the angle ϕ should be defined for the grid point. By extending the classification in such a way, the operational weather forecaster could get additional information about the horizontal extent of the sea- or land-breeze circulations, which could be useful when predicting for example the movement of the sea-breeze front.

As noted in section 1, the method can also be applied to observational data of the wind profile at the coast. A field campaign aiming at capturing the sea or land breeze could potentially bring more knowledge on how the indexing could be optimized. Further, classifying the conditions based on the SBI or LBI can help in understanding processes related to the sea or land breeze, such as e.g., turbulent processes, development of internal boundary layers and studies on the sea-breeze front and horizontal gradients of meteorological variables, both along the coast and in the crosswise direction. One limitation with the proposed method is that only cases when the return flow is fully or partly opposing the 10-m wind are considered. As such, sea breezes masked by a stronger synoptic flow will not be identified. If these cases were to be included, it is likely that the relative occurrence of SBI given the LWT would increase in both cyclonic conditions and in pure directional flow. However, as shown in Fig. 11, strong synoptic winds do not necessarily imply that winds at different heights in the boundary layer cannot oppose each other, although the relative occurrence of SBI under such circumstances is low.

One way to rule out some of the false alarms could be to implement a time derivative condition related to the decrease of the height of the onshore boundary layer that is associated with the onset of a sea breeze. The height of the boundary layer could also be used as a guide for which model levels to include in the comparisons of wind direction as both the sea-breeze circulation and the land-breeze circulation should be

vertically constrained to occur within the boundary layer. Unfortunately, the height of the boundary layer was not stored in the archive of HARMONIE-AROME forecasts for the full time period analyzed in this study and thus this methodology had to be discarded. Further, it is also important to note that the structure of the atmospheric boundary layer in the NWP model strongly depends on both the modeling system as a whole and the selected schemes for processes in the boundary layer. Model levels 51–38 (corresponding to approximately 500–2000 m) that were used to determine the return flow for the SBI and levels 46–62 (100–900 m) used for the return flow for the LBI were selected as they match the typical height range of the circulations (see also section 2c). A slight extension or reduction of the height range would impact the number of events found; however, it is likely that the qualitative results in the general statistics (Fig. 9) would remain. Which model levels are optimal to include in the analysis is likely to be dependent on the NWP model applied and which part of the world is studied.

The height of the circulation, as well as the wind speeds, both at 10 m and at upper levels, could be used to scale the SBI and LBI, if those measures are of value for the application in mind. To extend and develop the method further, the integrated mass flow in both the onshore and offshore directions could be analyzed using a mass streamfunction (Holton 1990). Although most commonly used to study changes in the global meridional circulation, the function could be applied to mesoscale circulations such as the sea or land breeze, resulting in an index indicating the strength of the circulation taking both the wind speed and the density of the air into account.

As suggested in section 1, the SBI and LBI could be used to study, e.g., model errors in temperature or cloudiness in the coastal zone and errors in predicted wind power production for wind farms (both onshore and offshore) affected by the sea- or land-breeze circulation. A similar metric could also be developed to study the impact of changing wind direction with height (and the consequent loads) on wind turbines (see Lundquist 2021). The method could easily be applied to reanalysis data of sufficient horizontal and vertical resolution to allow for multidecadal analysis of occurrence of sea and land breezes (see also Bedoya-Valestt et al. 2022).

As commented in section 2a, the terminology SBI and LBI can be slightly misleading as the indices only are measures of the change of wind direction with height and how much of a resemblance the wind directions at a lower and upper level have with the fully developed "textbook" sea or land breeze. Physical aspects of sea- or land-breeze formation are not taken into account. However, as shown by the 5-yr statistics in Fig. 9, the indices track the typical seasonal and diurnal patterns that could be expected from sea- and land-breeze circulations in this area.

Moving from a single-column based classification system (to detect sea- and land-breeze circulations), the algorithm could be extended by including the difference in air temperature over land and over water, surface heat fluxes and vertical wind components (both onshore and offshore). Thermodynamic gradients, both in the horizontal and vertical, could be necessary to include in coastal areas that are prone to strong convection with a high degree of wind turning with height. In this study we wanted to investigate the possibility to identify sea- and land-breeze circulations in their most straightforward way, only using the change of one variable (the wind direction) with height. The added complexity of an extended method would most likely result in a more robust classification but would be more labor and/or computationally expensive.

The refinements suggested above are recommended if the method is to be applied to create sea- or land-breeze climatologies or when investigating systematic biases in the NWP model due to these mesoscale circulations. For the operational weather forecaster, the indices could provide valuable information in its current formulation, but to minimize the number of false alarms of when a sea breeze (or land breeze) is occurring, the refinements can also be implemented operationally. Further, machine learning algorithms could be trained to recognize sea- or land-breeze circulations in NWP model output. If the training data (e.g., a subjective classification by a meteorologist if there is sea or land breeze in an area) is of sufficient length and quality, and if the machine learning algorithm is well tuned, this nonlinear methodology could probably also outperform simpler methods (Bedoya-Valestt et al. 2022). A (global) manually classified sea-breeze dataset could be used as a benchmark for this and similar studies.

Finally, it is also important to note that the forecaster can analyze more variables from the NWP model than just the SBI or LBI when determining if a sea or land breeze is occurring. As mentioned in section 1, the indices summarize the information about the vertical profile of the wind without the forecaster having to study the profiles or wind maps at different heights individually. Similar to, e.g., a thunder probability index, also the SBI and LBI will have flaws, and the forecaster will learn by experience in which situations the indices can be trusted as good predictors of the sea or land breeze, as opposed to when the change in the wind direction with height is due to other reasons. The method could easily be applied to ensemble forecasts of sufficient resolution to give a probabilistic assessment of the occurrence of a sea or land breeze.

5. Summary and conclusions

A new method to classify sea- and land-breeze circulations in NWP model output of sufficient resolution to resolve mesoscale phenomena in the coastal zone has been introduced and tested, with promising results. The HARMONIE-AROME model can capture coastal circulations well, which can clearly be seen both by studying maps of forecast cloud cover compared to satellite images (Fig. 4) and vertical cross sections of the wind field (Fig. 5).

Although simple and straightforward in its formulation (using only the direction of the coastline and the wind directions at 10 m and at upper levels in the column above one coastal grid point), the SBI and the LBI capture the expected seasonal and diurnal cycles of sea and land breezes for seven coastal sites in southern Sweden (Fig. 9). However, the main challenges for the method are in areas where the coastline is

complex, e.g., close to narrow straits, and cases with frontal passages associated with pronounced wind turning with height. Several suggestions to improve the method were discussed, among them limiting the allowed wind directions relative to the coastline, implementing time derivatives of the evolution of the height of the boundary layer, and scaling the indices by the wind speed and height of the circulation.

With an operational implementation of the SBI and LBI, the work of a weather forecaster could be simplified and possibly lead to an improved understanding of the weather situation and better communication with media and other stakeholders. The indices could also be presented in mobile phone applications together with the weather forecast, presenting valuable information for seafarers and people living at the coast. Further, the proposed indices could be used to create climatologies of the occurrence of sea and land breezes and as selection criteria to analyze forecast errors in the coastal zone.

Acknowledgments. We acknowledge the use of satellite imagery from the Worldview Snapshots application (https://wvs.earthdata.nasa.gov), part of the Earth Observing System Data and Information System (EOSDIS). This research has been supported by the Energimyndigheten VindEl program (Grant 47054-1). The work forms part of the Swedish strategic research program STandUP for Wind.

Data availability statement. The HARMONIE-AROME data used in the study were provided by the Norwegian Meteorological Institute (https://thredds.met.no/thredds/catalog.html).

REFERENCES

Banta, R. M., and Coauthors, 2020: Characterizing NWP model errors using Doppler-lidar measurements of recurrent regional diurnal flows: Marine-air intrusions into the Columbia River basin. *Mon. Wea. Rev.*, **148**, 929–953, https://doi.org/10.1175/MWR-D-19-0188.1.

Bedoya-Valestt, S., and Coauthors, 2022: A deep learning approach for identifying coastal sea breezes globally. *EMS Annual Meeting 2022*, Bonn, Germany, European Meteorological Society, Abstract EMS2022-522, Vol. 19, https://doi.org/10.5194/ems2022-522.

Bengtsson, L., and Coauthors, 2017: The HARMONIE–AROME model configuration in the ALADIN–HIRLAM NWP system. *Mon. Wea. Rev.*, **145**, 1919–1935, https://doi.org/10.1175/MWR-D-16-0417.1.

Biggs, W. G., and M. E. Graves, 1962: A lake breeze index. *J. Appl. Meteor.*, **1**, 474–480, https://doi.org/10.1175/1520-0450(1962)001<0474:ALBI>2.0.CO;2.

Borne, K., D. Chen, and M. Nunez, 1998: A method for finding sea breeze days under stable synoptic conditions and its application to the Swedish west coast. *Int. J. Climatol.*, **18**, 901–914, https://doi.org/10.1002/(SICI)1097-0088(19980630)18:8<901::AID-JOC295>3.0.CO;2-F.

Corpetti, T., and O. Planchon, 2011: Front detection on satellite images based on wavelet and evidence theory: Application to the sea breeze fronts. *Remote Sens. Environ.*, **115**, 306–324, https://doi.org/10.1016/j.rse.2010.09.003.

Crosman, E. T., and J. D. Horel, 2010: Sea and lake breezes: A review of numerical studies. *Bound.-Layer Meteor.*, **137**, 1–29, https://doi.org/10.1007/s10546-010-9517-9.

Eager, R. E., S. Raman, A. Wootten, D. L. Westphal, J. S. Reid, and A. Al Mandoos, 2008: A climatological study of the sea and land breezes in the Arabian Gulf region. *J. Geophys. Res.*, **113**, D15106, https://doi.org/10.1029/2007JD009710.

Feliks, Y., 1993: A numerical model for estimation of the diurnal fluctuation of the inversion height due to a sea breeze. *Bound.-Layer Meteor.*, **62**, 151–161, https://doi.org/10.1007/BF00705552.

Fernández-Granja, J. A., S. Brands, J. Bedia, A. Casanueva, and J. Fernández, 2023: Exploring the limits of the Jenkinson–Collison weather types classification scheme: A global assessment based on various reanalyses. *Climate Dyn.*, https://doi.org/10.1007/s00382-022-06658-7, in press.

Frysinger, J. R., B. L. Lindner, and S. L. Brueske, 2003: A statistical sea-breeze prediction algorithm for Charleston, South Carolina. *Wea. Forecasting*, **18**, 614–625, https://doi.org/10.1175/1520-0434(2003)018<0614:ASSPAF>2.0.CO;2.

Furberg, M., D. Steyn, and M. Baldi, 2002: The climatology of sea breezes on Sardinia. *Int. J. Climatol.*, **22**, 917–932, https://doi.org/10.1002/joc.780.

Gustavsson, T., S. Lindqvist, K. Borne, and J. Bogren, 1995: A study of sea and land breezes in an archipelago on the west coast of Sweden. *Int. J. Climatol.*, **15**, 785–800, https://doi.org/10.1002/joc.3370150706.

Hadi, T. W., T. Horinouchi, T. Tsuda, H. Hashiguchi, and S. Fukao, 2002: Sea-breeze circulation over Jakarta, Indonesia: A climatology based on boundary layer radar observations. *Mon. Wea. Rev.*, **130**, 2153–2166, https://doi.org/10.1175/1520-0493(2002)130%3C2153:SBCOJI%3E2.0.CO;2.

Hersbach, H., and Coauthors, 2020: The ERA5 global reanalysis. *Quart. J. Roy. Meteor. Soc.*, **146**, 1999–2049, https://doi.org/10.1002/qj.3803.

Holmer, B., and M. Haeger-Eugensson, 1999: Winter land breeze in a high latitude complex coastal area. *Phys. Geogr.*, **20**, 152–172, https://doi.org/10.1080/02723646.1999.10642674.

Holton, J., 1990: On the global exchange of mass between the stratosphere and troposphere. *J. Atmos. Sci.*, **47**, 392–395, https://doi.org/10.1175/1520-0469(1990)047<0392:OTGEOM>2.0.CO;2.

Jenkinson, A., and F. Collison, 1977: An initial climatology of gales over the North Sea. Synoptic Climatology Branch Memo. 62, Meteorological Office, 18 pp.

Jones, P., C. Harpham, and K. Briffa, 2012: Lamb weather types derived from reanalysis products. *Int. J. Climatol.*, **33**, 1129–1139, https://doi.org/10.1002/joc.3498.

Kalverla, P. C., J. B. Duncan Jr., G.-J. Steeneveld, and A. A. Holtslag, 2019: Low-level jets over the North Sea based on ERA5 and observations: Together they do better. *Wind Energy Sci.*, **4**, 193–209, https://doi.org/10.5194/wes-4-193-2019.

Kambezidis, H., D. Weidauer, D. Melas, and M. Ulbricht, 1998: Air quality in the Athens basin during sea breeze and non-sea breeze days using laser-remote-sensing technique. *Atmos. Environ.*, **32**, 2173–2182, https://doi.org/10.1016/S1352-2310(97)00409-3.

Lamb, H. H., 1972: British Isles weather types and a register of the daily sequence of circulation patterns 1861-1971. *Geophysical Memoirs*, HMSO, 85 pp.

Lundquist, J. K., 2021: Wind shear and wind veer effects on wind turbines. *Handbook of Wind Energy Aerodynamics*, B. Stoevesandt

et al., Eds., Springer International Publishing, 1–22, https://doi.org/10.1007/978-3-030-05455-7_44-1.

Lyons, W. A., 1972: The climatology and prediction of the Chicago lake breeze. *J. Appl. Meteor.*, **11**, 1259–1270, https://doi.org/10.1175/1520-0450(1972)011<1259:TCAPOT>2.0.CO;2.

Miao, J.-F., L. Kroon, J. Vilà-Guerau de Arellano, and A. Holtslag, 2003: Impacts of topography and land degradation on the sea breeze over eastern Spain. *Meteor. Atmos. Phys.*, **84**, 157–170, https://doi.org/10.1007/s00703-002-0579-1.

Miller, S., B. Keim, R. Talbot, and H. Mao, 2003: Sea breeze: Structure, forecasting, and impacts. *Rev. Geophys.*, **41**, 1011, https://doi.org/10.1029/2003RG000124.

Neumann, J., 1977: On the rotation rate of the direction of sea and land breezes. *J. Atmos. Sci.*, **34**, 1913–1917, https://doi.org/10.1175/1520-0469(1977)034<1913:OTRROT>2.0.CO;2.

Physick, W., and R. Byron-Scott, 1977: Observations of the sea breeze in the vicinity of a Gulf. *Weather*, **32**, 373–381, https://doi.org/10.1002/j.1477-8696.1977.tb04481.x.

Planchon, O., F. Damato, V. Dubreuil, and P. Gouéry, 2006: A method of identifying and locating sea-breeze fronts in northeastern Brazil by remote sensing. *Meteor. Appl.*, **13**, 225–234, https://doi.org/10.1017/S1350482706002283.

Porson, A., D. G. Steyn, and G. Schayes, 2007: Formulation of an index for sea breezes in opposing winds. *J. Appl. Meteor. Climatol.*, **46**, 1257–1263, https://doi.org/10.1175/JAM2525.1.

Prtenjak, M. T., and B. Grisogono, 2007: Sea/land breeze climatological characteristics along the northern Croatian Adriatic coast. *Theor. Appl. Climatol.*, **90**, 201–215, https://doi.org/10.1007/s00704-006-0286-9.

Roy, S., A. Sentchev, M. Fourmentin, and P. Augustin, 2022: Machine learning and deterministic methods for detection meteorological phenomena from ground measurements: Application for low-level jet and sea-breeze identification in northern France. *Atmosphere*, **13**, 1873, https://doi.org/10.3390/atmos13111873.

Sills, D. M. L., J. R. Brook, I. Levy, P. A. Makar, J. Zhang, and P. A. Taylor, 2011: Lake breezes in the southern Great Lakes region and their influence during BAQS-Met 2007. *Atmos. Chem. Phys.*, **11**, 7955–7973, https://doi.org/10.5194/acp-11-7955-2011.

Simpson, J. E., 1994: *Sea Breeze and Local Winds*. Cambridge University Press, 234 pp.

Sokolov, A., E. Dmitriev, C. Gengembre, and H. Delbarre, 2020: Automated classification of regional meteorological events in a coastal area using in situ measurements. *J. Atmos. Oceanic Technol.*, **37**, 723–739, https://doi.org/10.1175/JTECH-D-19-0120.1.

Steele, C., S. Dorling, R. von Glasow, and J. Bacon, 2015: Modelling sea-breeze climatologies and interactions on coasts in the southern North Sea: Implications for offshore wind energy. *Quart. J. Roy. Meteor. Soc.*, **141**, 1821–1835, https://doi.org/10.1002/qj.2484.

Svensson, N., H. Bergström, A. Rutgersson, and E. Sahlée, 2019: Modification of the Baltic Sea wind field by land-sea interaction. *Wind Energy*, **22**, 764–779, https://doi.org/10.1002/we.2320.

Talbot, C., P. Augustin, C. Leroy, V. Willart, H. Delbarre, and G. Khomenko, 2007: Impact of a sea breeze on the boundary-layer dynamics and the atmospheric stratification in a coastal area of the North Sea. *Bound.-Layer Meteor.*, **125**, 133–154, https://doi.org/10.1007/s10546-007-9185-6.

Vignes, O., 2021: MetCoOp status and plans. Norwegian Meteorological Institute, 1 p., https://www.umr-cnrm.fr/accord/IMG/pdf/metcoop_status_asw21_olev.pdf.

Wakimoto, R. M., and N. T. Atkins, 1994: Observations of the sea-breeze front during CaPE. Part I: Single-Doppler, satellite, and cloud photogrammetry analysis. *Mon. Wea. Rev.*, **122**, 1092–1114, https://doi.org/10.1175/1520-0493(1994)122<1092:OOTSBF>2.0.CO;2.

Wentworth, G., J. Murphy, and D. Sills, 2015: Impact of lake breezes on ozone and nitrogen oxides in the Greater Toronto Area. *Atmos. Environ.*, **109**, 52–60, https://doi.org/10.1016/j.atmosenv.2015.03.002.

Wilcke, R. A. I., E. Kjellström, C. Lin, D. Matei, A. Moberg, and E. Tyrlis, 2020: The extremely warm summer of 2018 in Sweden—Set in a historical context. *Earth Syst. Dyn.*, **11**, 1107–1121, https://doi.org/10.5194/esd-11-1107-2020.

Xia, G., C. Draxl, M. Optis, and S. Redfern, 2022: Detecting and characterizing simulated sea breezes over the U.S. northeastern coast with implications for offshore wind energy. *Wind Energy Sci.*, **7**, 815–829, https://doi.org/10.5194/wes-7-815-2022.

Yiou, P., and Coauthors, 2020: Analyses of the northern European summer heatwave of 2018. *Bull. Amer. Meteor. Soc.*, **101**, S35–S40, https://doi.org/10.1175/BAMS-D-19-0170.1.